Structure dependence of molecular reactions on surfaces

Cao, K.

Chapter 4

Hydrogen adsorption and desorption from Cu(111) and Cu(211)

4.1 Introduction

Few chemical reactions occurring at the gas-surface interface have been studied with similar intensity as hydrogen dissociation on Cu. It serves as the model system for strongly activated dissociative adsorption of a simple diatomic molecule on a metal surface [18, 34]. In recent years, however, it has also become of practical importance. The industrial hydrogenation of CO_2 to methanol over a $Cu/ZnO/Al_2O_3$ catalyst, is considered to be rate-determined by elementary hydrogenation steps involving dissociated hydrogen[46–48]. The industrial process presents a potential means to fixate CO_2. However, it currently suffers from high pressure and moderate temperature requirements[46]. A thorough understanding of all elementary reaction steps involved may advance the development of new catalysts that operate at less energy-consuming conditions. The dissociation of molecular hydrogen on (defective) Cu surfaces is such an elementary step that is crucial to the reaction.

Using supersonic molecular beam (SMB) methods and temperature programmed desorption (TPD), Anger, Winkler, and Rendulic showed for low Miller surfaces that the reactivity order toward H_2 dissociation is Cu(111) > Cu(100) > Cu(110)[49]. Sakong and Groß reproduced this trend in a theoretical study of atomic hydrogen adsorption and H_2 dissociation[50]. For the most intensely studied Cu(111) surface

in this context, Winkler's group also initiated studies on vibrational effects to hydrogen dissociation [51]. Auerbach, Rettner and Michelsen subsequently combined SMB, permeation and laser-based techniques to study adsorption and desorption in a state-specific manner[52–59]. Their studies showed, amongst others, that the vibrational motion plays a large role in the dissociative adsorption. They also demonstrated the applicability of the principle of detailed balance, that is, that adsorption and desorption experiments are similarly accurate at determining important kinetic and thermodynamic quantities of the reaction. In the same decade, Darling and Holloway carried out a series of theoretical studies on rotational, vibrational, and surface temperature effects to dissociative adsorption[40, 60–63]. While they could achieve qualitative agreement with experimental results on the importance of individual molecular degrees of freedom for the dynamics, an acceptable quantitative agreement regarding absolute reactivities was, however, then not attainable. More recently, Díaz et al. continued theoretical studies based on the specific reaction parameter (SRP) approach to density functional theory (DFT)[34, 64]. Their dynamics calculations performed for the H_2 + Cu(111) system accurately reproduced experimental results on sticking, the effect of molecular vibrational and rotational motion on dissociative adsorption and associative desorption, and the amount of rotational excitation of scattered molecules.

Experimental studies of the influence of defects on H_2 dissociation on Cu are sparse. In an early study, Balooch et al. observed that the highly corrugated Cu(310) surface does not exhibit higher HD yields than the Cu(100) surface when exposed to molecular hydrogen and atomic deuterium[65]. They suggested that the edges on this stepped surface are not the principal regions for H_2 adsorption. Theoretical studies performed on similar systems have found the opposite. Using an embedded-atom method (EAM) and a cluster of 800 Cu atoms, Liao and Sun computed a significant decrease for the H_2 dissociative barrier for the Cu(410) plane in comparison to the Cu(100) plane [66]. Šljivančanin and Hammer performed calculations on the reaction barrier for H_2 dissociation on Cu surfaces constructed from the most narrow (111) terrace with A- and B-type steps, that is, Cu(211) and Cu(221), for kinks in step edges, and for vacancy sites in the Cu(111) plane[67]. They found that all types of defects lowered the H_2 dissociation barrier in comparison to the flat Cu(111) surface. A

reduced dissociation barrier for Cu(211) compared to Cu(111) was also predicted by calculations of Behrens et al. based on density functional theory (DFT) that focused on the mechanism of CO_2 hydrogenation [48]. Such increased reactivity for stepped metal surfaces is often rationalized using the d-band theory[68, 69], the important parameter being the position of the d-band relative to the Fermi level.

Recently, we have co-authored a combined theoretical and experimental study on the reactivity of D_2 on clean Cu(211) and Cu(111) surfaces at zero-coverage[70]. Based on ∼115,000 DFT energy points calculated using the SRP48 functional[71], a new potential energy surface (PES) was constructed for the H_2 + Cu(211) system. Surprisingly, subsequently performed molecular dynamics simulations using this PES showed in agreement with new SMB measurements that hydrogen dissociation is more likely on the flat Cu(111) surface than on the stepped Cu(211) surface. The observed lower reactivity of the stepped surface for bond cleavage of molecular hydrogen was rationalized by somewhat larger reaction barriers that were computed for H_2 + Cu(211) and the overall increased complexity of the underlying gas-surface interaction potential in comparison to the H_2 + Cu(111) system.

In the following, we present an experimentally more comprehensive set of data obtained using a combination of SMB techniques and TPD for Cu(211) and Cu(111). The former is a highly corrugated surface with 3-atom wide (111) terraces, which are separated by the monoatomic steps representing a (100) facet. They are also referred to as A-type steps. The additional TPD experiments not only allow us to extend the range of detectable probabilities for dissociative adsorption, we also infer activation barriers to desorption, their surface coverage dependence, and a relation between the obtained saturation coverage and incident energy. Our experimental data is supplemented by additional periodic DFT calculations that probe how the activation barrier energy is modified by different surface concentrations of atomic hydrogen pre-adsorbed on the two different surface facets. Our results contribute to the present knowledge regarding the effect of steps and defects on the reaction dynamics of gas-surface systems.

4.2 Experimental and theoretical methods

4.2.1 Molecular beam apparatus and experimental methodology

All experiments were carried out using a home-built UHV system with a base pressure below 8×10^{-11} mbar. The main UHV chamber is connected to a series of vacuum chambers used to generate a well-defined molecular beam through supersonic expansion of molecular hydrogen (deuterium). We use as our expansion nozzle a 25 μm diameter orifice, laser drilled through the flat end wall of a hollowed single crystalline tungsten rod. This tungsten tip is laser welded to a 100 mm long tantalum tube which is held at the opposite end by a large stainless steel block suspended from an *x, y, z* manipulator. The nozzle's 25 μm diameter orifice is accurately positioned at variable distance (between approx. 1 and 15 mm) from the first of this series of skimmers (Model 1, 0.25 mm, Beam Dynamics). We create the supersonic expansion into vacuum by flowing gases from a gas manifold using flow controllers and pressures between 1 and 5 bara into the Ta-W tube. To increase the kinetic energy of molecules in the expansion, the tungsten tip of the nozzle is heated radiatively by a second short tungsten tube that surrounds the tungsten tip. This second tube is heated by electron bombardment using two oppositely positioned filaments. A C-type thermocouple is spot welded to the Ta part of the expansion tube, approx. 10-20 mm from the 25 μm diameter orifice. A strong thermal gradient along the expansion tube leads to a temperature reading for the nozzle, T_n, below the actual temperature at the orifice.

We skim the gas expansion in the source chamber to create a beam which passes through two stages of differential-pumping prior to entering the UHV chamber, which houses a temperature-controlled Cu single crystal on an *x, y, z,* θ manipulator. A valve separates the two differential pumping stages. When closed, the background pressures for H_2 and D_2 in the main chamber are determined. Two additional flags in the beam line can be opened and closed. They are used to determine the absolute dissociation probabilities by the King and Wells (KW) technique[10]. For KW measurements, we use a Baltzers quadrupole mass analyzer (QMA200), positioned such that it samples the pressure rise from the SMB after equilibration inside the chamber. The first

flag is located in the first differential pumping stage. When closed, the effusive load of the beam onto the main UHV chamber can be determined. As a second flag, we use a wheel located inside the main UHV chamber. It has a 50% duty cycle divided over two "open" sections of equal size. It is firmly attached to the axis of a UHV-compatible stepper motor (Arun Microelectronics) and used, here, only to control impingement of the beam onto the crystal within the UHV chamber in an "on/off" fashion by a single, step-wise rotation of the wheel over one quarter turn. The opening and closing of both flags is computer-controlled to ensure an accurate timing. When retracting the sample, the beam enters the differentially-pumped housing of a Baltzer's 400 quadrupole mass analyzer (QMA400) of a special linear design with a cross-beam ionizer and two consecutive quadrupole mass filters. It is used to determine the kinetic energy of molecules in the beam through time-of-flight (TOF) analysis and for TPD. The differentially-pumped QMA is retractable over 200 mm along the beam axis, allowing TOF measurements for varying neutral flight path lengths. The kinetic energy distribution of molecules in each SMB used to determine sticking probabilities is determined as described in detail in the Supporting Information of Ref. [70]. For the analysis, we assume the standard form for a flux-weighted velocity distribution and take into account that our QMA ionizer is a density-sensitive detector. We also incorporate the chopper function in the fitting procedure. More details of our entire UHV-SMB system were previously described in Ref.[11].

In this work, we use two copper single crystals exposing polished (111) and (211) surfaces. They are 10 mm in diameter, 1 mm thick, of 6N purity, and aligned to $< 0.1^\circ$ from the indicated surface (Surface Preparation Laboratory, Zaandam, The Netherlands). They can be heated at least up to 900 K by electron bombardment heating. They can be cooled to 90 K using liquid nitrogen. The Cu crystals are attached to the sample holder in a way that allows us to adjust the azimuthal angle with an accuracy $\sim 2^\circ$. The polar angle of incidence may be changed up to $\sim 60^\circ$ with an accuracy of $\sim 0.5^\circ$. The surface structure and azimuthal orientation were verified by low energy electron diffraction (LEED). The spot-splitting to row-spacing ratio for the (211) surface was found to be 2.47, in very good agreement with the expected value of 2.45[72]. Cleanliness is checked regularly using Auger electron spectroscopy (AES) (OCI Vacuum, BDL800IR-MCP). Cleaning procedures were identical for both surfaces. We use repetitive

cycles of argon ion sputtering at a surface temperature (T_s) of 400 K and at normal incidence (10 minutes, ~ 1 μA) with subsequent annealing at $T_s = 800$ K for another 10 minutes. This procedure is repeated at least three times before experiments were performed. We combined each measurement of the absolute dissociation probability, S, with a subsequent TPD measurement. We then heated the Cu crystal to 800 K to remove adsorbates. For beam conditions that lead to dissociation probabilities near or below our detection limit, we determine the initial dissociation probability, S_0, by averaging up to 10 independent measurements. This reduces our KW detection limit for S_0 to ~ 0.005. To determine even lower dissociation probabilities, we use the integrated signal of TPD spectra as discussed in detail in the Results section given below.

TPD spectra are taken after exposing the surface to $H_2(D_2)$ for a well-defined time using the molecular beam. In this work, we solely report on TPD spectra from dosing using the SMB - the reactivity is too low to achieve comparable surface coverages from background dosed hydrogen applied at acceptable pressures and exposure times. Dissociative adsorption was probed at normal incidence of the molecular beam and all TPD spectra were taken with the QMA's axis aligned with the crystal's surface normal. The SMBs were generated using pure H_2 (6N, Linde Gas, Rotterdam, The Netherlands) or pure D_2 (2N8 isotopic purity, Linde Gas, Rotterdam, The Netherlands) without further treatment. The rate of heating for all reported TPD spectra was determined to be 2.0 K s^{-1}. The distance between the Cu crystal's polished surface and the 3.0 mm diameter aperture of the QMA housing is kept constant at ~ 2 mm. The reduced pumping speed in between the crystal's surface and the aperture, and the low pumping speed surrounding the QMA's ionizer inside its differential housing, allows this configuration to be taken to be (near) angle-integrating.

4.2.2 Computational methodology

Periodic DFT calculations were carried out using the Vienna ab initio simulation package (VASP)[73–76] and the SRP48-functional. We are particularly interested in changes of the classical activation energy for the dissociation of H_2 on Cu(111) and Cu(211) caused by the presence of pre-adsorbed hydrogen atoms at coverages of 1/9 and 2/9 ML. For calculations on the H_2 + Cu(111) system,we chose a (3×3) supercell

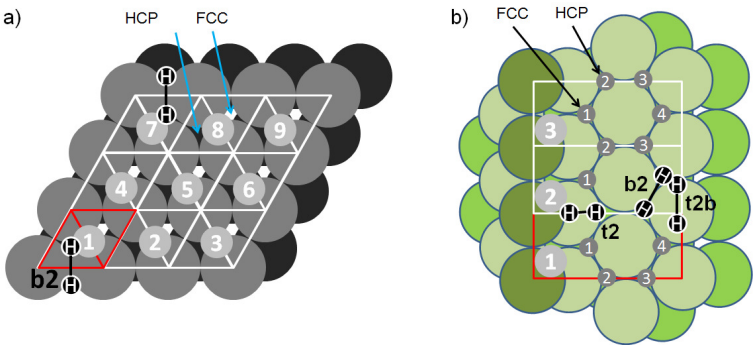

Figure 4.1: Shown are in a) the (3×3) supercell for Cu(111) and in b) the (3×1) supercell for Cu(211) as used in the calculations. Light grey filled circles with numbers label the different unit cells. In b), smaller darker grey circles with numbers indicate H_{ads} positions. Also indicated in black stick models are the geometries of transient H_2 molecules assumed at the different barriers that were considered in this work, i.e. the b_2 site for Cu(111) and the t_2, b_2, and t_2b sites for Cu(211).

and a k-point mesh of $6 \times 6 \times 1$. Further details on the slab model and the applied computational setup are given in ref.[71]. Calculations on H_2 + Cu(211) were performed using a (3×1) supercell and the same 5 layer slab model and the same computational setup as described in Ref. [70]. The supercells are shown in figure 4.1 as well as the corresponding smallest unit cells distinguished by the numbers embedded in the gray circles.

To compute the coverage dependence of the activation barrier we proceed as follows. For the Cu(111) surface, we place the transient H_2 molecule at the transition state geometry specified in Ref.[77] and indicated in figure 4.1a) at the b_2 site. In the case of Cu(211), we select the geometries of transient H_2 associated with the barriers at the b_2, t_2 and t_2b sites, which we have previously found to play an important role in the dissociation process[70]. The corresponding H_2 geometries are also indicated in figure 4.1b). Coverages of 1/9 ML on Cu(111) were simulated by placing a single hydrogen atom in one out of the nine unit cells at either the FCC or the HCP position, see figure 4.1a). We neglect situations in which H_{ads} would lead to strong repulsive interactions with the H_2 molecule and have therefore not considered coverage-configurations over the unit cells 1 and 7 of Cu(111), see figure 4.1a). On Cu(211), we proceed similarly and put H_{ads} at selected local minima in a manner that repulsive interactions with transient H_2 are kept small. According to our DFT calculations,

the four different minima for hydrogen atom adsorption on Cu(211) as indicated by encircled numbers in figure 1b) follow the stabilization order $4 > 3 > 2 > 1$ whereby the hollow site located near the step edge, i.e. site 4, is the preferred adsorption site for a single hydrogen atom. To simulate coverages of 2/9 ML, we placed another H_{ads} at a proper position on the supercell while carefully avoiding too large H_{ads}-H_2 and H_{ads}-H_{ads} repulsions. This procedure leads to pre-covered surfaces of different surface structures that have all been considered in the calculations. The computed reaction barriers therefore vary within a certain energy range, and effective barriers represent averages over all barriers calculated for the different adsorbate layer structures. The calculated reaction barrier energies are given with respect to the potential energy that the system assumes when the H_2 molecule is moved to the gas phase (here 6 Å away from the Cu-surfaces) at its classical equilibrium position (H-H distance is ∼0.74 Å). We note that the considered reaction barrier geometries were not reoptimized in the presence of pre-adsorbed hydrogen. Normal mode analyses rigorously performed for almost all the different coverage configurations revealed that the barriers toward H_2 dissociation considered here remained first order saddle points. This makes the approach of using fixed TS geometries reliable in the computation of the coverage dependence of the activation energies.

4.3 Results

4.3.1 Initial dissociation probability by the King and Wells method

In figures 4.2a) and 4.2b), we exemplify our procedure to determine S_0 at conditions where the sticking probability is too low to be accurately determined by a single KW measurement. Note that the QMA signal in figure 4.2a) shows only the upper 10% of the relative increase in hydrogen partial pressure when the molecular beam enters the main UHV chamber. Inset I of figure 4.2a) shows a single measurement plotted over the entire QMA signal. The data is normalized and corrected for the background pressure of molecular hydrogen present in the main UHV chamber. Data presented as a solid black line in the main plot of panel a) represent the average of multiple measurements shown in

red. One can see that the small dip appearing at 16 s - the moment in which the exposure of the surface to H_2 starts - can only be resolved after averaging multiple measurements and proper magnification of the averaged signal.

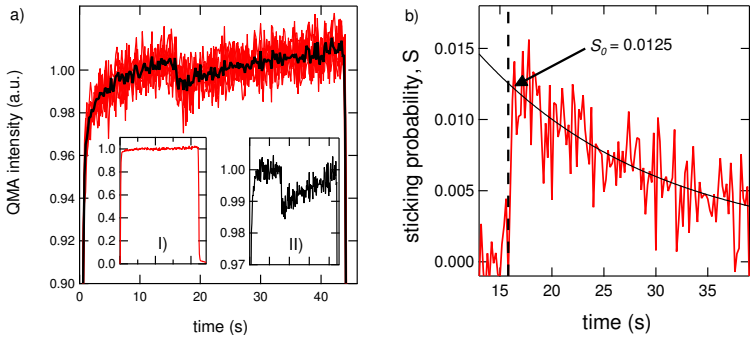

Figure 4.2: Illustration of the applied procedure to determine dissociative sticking of H_2 on Cu(111) by the King and Wells technique. Recorded QMA signals as function of the exposure time are plotted in panel a). Red curves show ten independent KW measurements. The black curve is the corresponding average result. The main panel shows the upper 10% of the full range of the normalized QMA intensity change when admitting the SMB to the UHV chamber. In inset I, the time-dependence of a single measurement is shown over the full range. Inset II shows the average signal after correcting for the change in QMA sensitivity resulting from reduction of the channeltron's inner surface. Panel b) shows the sticking probability, S, as a function of exposure time. The solid black curve is a fit to the data used to extract the indicated value of S_0 at the time of opening the beam flag. The latter is indicated by a vertical dashed line.

We subsequently correct for the small but noticeable increase of the hydrogen partial pressure over longer times. The small continuing rise is hardly noticeable in inset I, but is clearly visible in the top 10% of the pressure versus time trace. We do not believe that it represents an actual partial pressure rise, e.g. generated by slow equilibration of poorly pumped spaces in the UHV chamber. The time constant of the gradual change is too long. Instead, we attribute it to improving amplification of the QMA's channeltron through reduction of its inner surface by exposure to the reducing gas, H_2. We have observed the opposite effect in a study on the dissociation of O_2 dissociation on Pd(100) using the same type of QMA[14]. We correct for this increase in QMA sensitivity by fitting the time-dependent pressure using an exponential form and dividing the data by this exposure-dependent sensitivity function. In the fitting procedure, we mask the part of the data near the dip in

pressure resulting from dissociative adsorption. We have verified that the change in QMA sensitivity is consistent over multiple days and that the fitting function used here reproduces the pressure versus time trace recorded at conditions leading to no discernible dissociation. The upper 10% of the resulting corrected trace is shown in inset II of figure 4.2a). We finally invert the signal and fit the dissociation probability over time. The fit is of a double-exponential form and shown in figure 4.2b) as a black trace. The latter procedure reduces small errors introduced by the convolution of the actual time-resolved dissociation probability, $S(t)$, with the time constants for opening the second shutter and the gating time of QMA data collection. We estimate that the so-determined S_0 values are accurate to at least two significant figures.

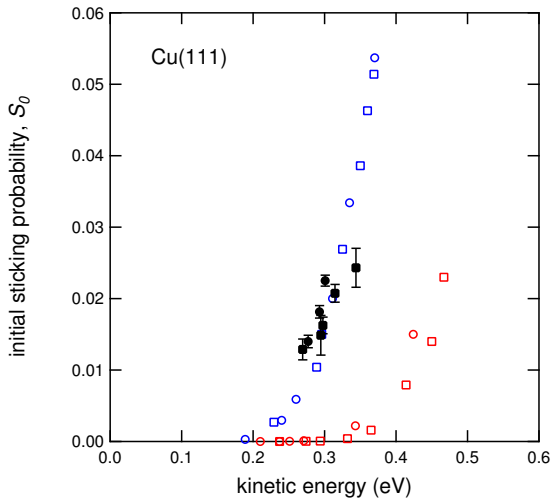

Figure 4.3: Initial sticking probability data for for D_2 (squares) and H_2 (circles) dissociation on Cu(111) from refs. [49, 51] (open blue) and [53, 78] (open red) and current data (solid black) as a function of incident kinetic energy. Error bars reflect the uncertainty from the time-dependent fit as described in figure 4.2b). Kinetic energy for current data represents the most probable kinetic energy from TOF fitting, whereas [53, 78] imply the average kinetic energy.

Figure 4.3 compares our initial sticking probability data for D_2 on Cu(111) to data published previously for dissociative sticking of hydrogen and deuterium to this surface [51, 53, 78]. Our data are shown versus the most probable energy of the energy distribution as determined by time-of-flight and indicated by squares. Error bars reflect the uncertainty in the fit of time vs S traces as shown in figure 4.2b). As

will be shown below, the energy distributions in our beams are rather broad, especially when using high nozzle temperatures. The data published by Berger et al. for H_2 (open blue circles) and D_2 (open blue squares) unfortunately lack a definition of their energy axis, although they indicate that the kinetic energies of their beams were determined using time-of-flight techniques. They do not show typical results for an energy distribution, but specify that the energy is $\sim 5kT_n/2$, with k being Boltzmann's constant. Rettner and Auerbach published time-of-flight spectra [79] and indicated 2.65k as the linear scaling factor between energy and nozzle temperature[52]. Their data for H_2 (open red circles) and D_2 (open red squares) are shown versus the mean energy of their characterized beams. While our data agrees rather well with those from Berger et al., they are clearly considerably higher than those from Auerbach and coworkers. In the Discussion section, we explain the origin of this apparent discrepancy.

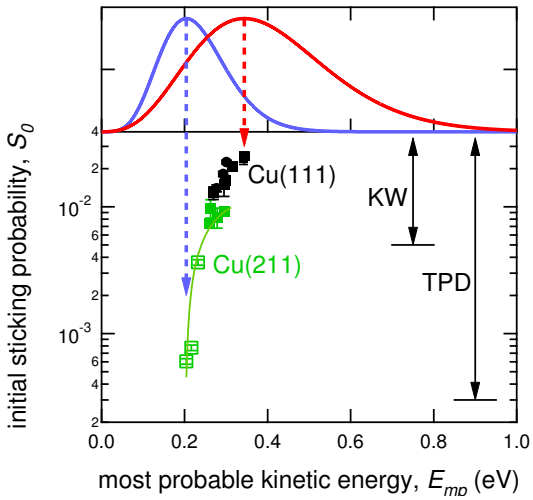

Figure 4.4: The top panel shows two energy distributions obtained from TOF analyses for two representative pure D_2 beams obtained at different nozzle temperatures. Their most probable energies E_{mp} are indicated by the vertical dashed lines. The bottom panel plots initial sticking coefficients, S_0, for H_2 (circles) and D_2 (squares) as function of E_{mp} for Cu(111) (black filled symbols) and for Cu(211) (open green symbols). The range over which absolute reactivity is determined by KW measurements is indicate by a vertical bar in the lower panel. Relative values were established with TPD measurements over the range indicated also by a vertical bar. The solid green line in the bottom panel is a fit of exponential functional form to the data for D_2 dissociation on Cu(211) serving to guide they eye.

Figure 4.4 compares our absolute dissociative sticking probabilities of D_2 (H_2) for Cu(111) as plotted in figure 4.3 to Cu(211). To illustrate that our measurements are not energy-resolved, we show in the upper panel of figure 4.4 two kinetic energy distributions for pure D_2 beams generated at different nozzle temperatures. We previously reported a linear relation between the kinetic energy and nozzle temperature with 2.53k as the scaling factor for our molecular beam system.[45] As we have lost the ability to measure the actual expansion temperature due to changes in the nozzle design, we cannot determine the scaling factor. However, the energy distributions are very similar to those obtained earlier for similar expansion conditions and assuming only an offset in the temperature measurement. In the lower panel of figure 4.4, we plot initial sticking coefficients versus the most probable kinetic energy, E_{mp}, of the associated molecular beams. For H_2 and D_2 impacting on Cu(111) we again use black circles and squares, respectively. For D_2 dissociation on Cu(211), we have used solid green squares for data obtained by KW technique. Data determined by the KW method provides absolute values, but are limited to values larger than 0.005. These data serve to determine lower S_0 values obtained from integrated TPD spectra, as explained in detail below. The latter are shown as open green squares. The solid green line is an exponential fit to the data and included to guide the eye. The data in figure 4.4 show that the Cu(111) surface is significantly more reactive in dissociating hydrogen than Cu(211). The difference is approximately a factor of 2 in the regime where we have been able to collect data by the KW method reproducibly for both surfaces under identical expansion conditions.

We have attempted to widen the kinetic energy range over which we can determine S_0. Attempts to increase reactivity by seeding small amounts of D_2 in H_2 while expanding at the highest attainable nozzle temperatures failed. With abundant H_2, the tungsten tip of our nozzle converts nearly all D_2 into HD through reaction at its inner surface prior to expansion. It leaves too little D_2 in the gas mixture to allow KW measurement of S_0 at higher incidence energy. On the lower kinetic energy side, the limited flux of D_2 molecules in our molecular beam prevents detecting lower reactivities. Exposure times needed to obtain a measurable quantity of D_2 in TPD spectra became too long to guarantee surface cleanliness. For example, CO in the residual gas of our UHV system sticks to the Cu surfaces at the temperatures required for the molecular beam adsorption measurements.

Considering the width of the kinetic energy distributions in our beams and the significant difference in expansion temperatures required to vary the most probable kinetic energy in our experiments, the determined dissociation probabilities seem to be dominated by the high energy tail of the distribution and/or ro-vibrationally excited molecules. Although it is in principle possible to deconvolute the data in figure 4.4 for incident energy and vibrational state[53], we do not. The energy distributions in our beams are too broad, the measured temperature of the nozzle does not represent the actual expansion temperature, and our data set is too limited to yield reliable results. Therefore, we leave this data as qualitatively indicating the surprising result of lowered reactivity by introducing (100) type steps at a high density to the (111) surface, and try to reveal its origin using quantitative TPD.

4.3.2 Temperature programmed desorption

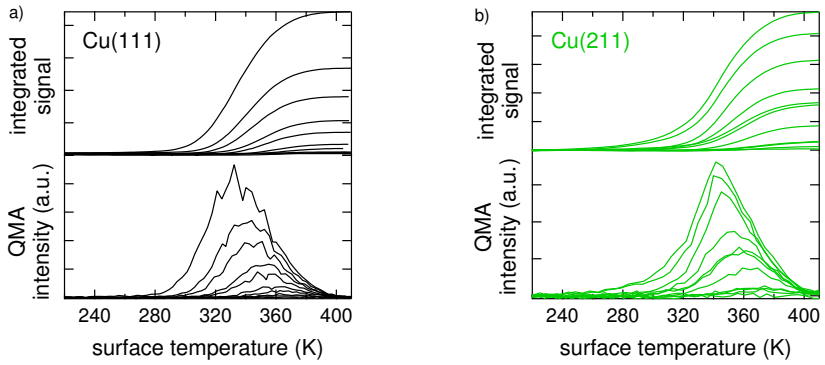

Figure 4.5: At the bottom, TPD spectra are shown for various pure D_2 molecular beam doses at T_s = 90 K onto a) Cu(111) and b) Cu(211) for E_{kin} = 0.298 eV. The integrated spectra are shown in the top panels.

Figure 4.5a) exemplifies background-subtracted D_2 TPD spectra (bottom) and the temperature-integrated spectra (top) for various doses from the molecular beam under fixed expansion conditions onto Cu(111) for a most probable beam energy of 0.298 eV. Figure 4.5b) shows the same for Cu(211) for the identical kinetic energy and energy distribution. The peak desorption temperature shifts for Cu(111) downward from $\sim$ 365 K to $\sim$ 330 K with increasing coverage. Trailing edges overlap mostly. The Cu(211) surface shows the same behavior for

desorption temperatures that are $\sim$ 10 K higher. Overlapping trailing edges are characteristic for second order desorption kinetics with negligible adsorbate-adsorbate interactions. For the highest doses, Cu(211) shows a clear shoulder developing at the low temperature side of the major desorption peak. The onset of desorption for the highest D-coverage is located around 260 K. Cu(111) shows no desorption in this temperature regime even after extended doses at the indicated kinetic energy.

The rate of thermal desorption is usually described by the Polanyi-Wigner equation, as equation (2.10) and equation (2.11) show in chapter 2.

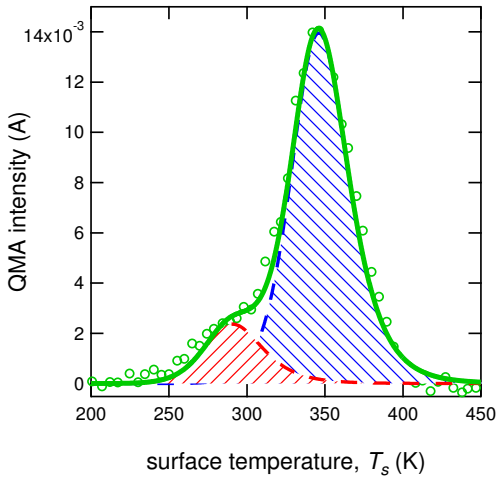

Figure 4.6: Runge-Kutta based simulation of an experimental D_2 TPD spectrum for Cu(211). Experimental data are shown as open circles. The solid green line equals the sum of two separate contributions. The parameters used for the main peak (dashed blue) are $E_{des} = 75.5$ kJ/mol, $\nu = 1 \times 10^{11}$ s^{-1}, $\theta_0 = 0.35$ ML, and $n = 2$. For the shoulder (dashed red), $E_{des} = 52$ kJ/mol, $\nu = 5 \times 10^9$ s^{-1}, $\theta_0 = 0.06$ ML, $n = 2$.

Quantitative analysis of TPD spectra is complex as both E_{des} and ν in equation (2.10) may depend on coverage. To obtain an estimate of the desorption energy for the main peak and shoulder observed at higher coverages for Cu(211), a TPD spectrum was initially simulated by solving equation (2.10) with the Runge-Kutta method. For the simulation, we assume that ν and E_{des} are independent of coverage. We also distribute the total initial coverage, θ_0, (here 0.41 ML) over the two apparent desorption peaks. Figure 4.6 shows the spectrum

with experimental data indicated by open circles. The red curve is the simulation of the shoulder peak and the blue curve the simulation of the main peak. The green curve is the summation of the two individual peaks. The parameters used for this simulation are $E_{des} = 75.5$ kJ/mol, $\nu = 1 \times 10^{11}\ s^{-1}$, $\theta_0 = 0.35$ ML, $n = 2$ and $E_{des} = 52$ kJ/mol, $\nu = 5 \times 10^{9}\ s^{-1}$, $\theta_0 = 0.06$ ML, $n = 2$ for the main peak and shoulder peak, respectively. Increasing E_{des} for the shoulder requires increasing ν in order to keep the simulation and TPD spectrum comparable. However, the width of the simulated shoulder visibly becomes too narrow in comparison to the TPD spectrum. With the indicated parameters, the shoulder peak's area is less than 15% of the total area. The desorption energy difference for the two peaks is approximately 23.5 kJ/mol.

Using the so-called 'complete analysis' method[17], we can determine E_{des} and ν for every coverage. It requires changing equation (2.10) into equation (2.12). An Arrhenius plot of ln r versus $1/T_s$ yields $-E_{des}/R$ as the slope. The intercept for any particular coverage equals ln $\nu(\theta) + n$ ln θ. Figure 4.7 exemplifies a subset of the results when applying this procedure to TPD spectra taken for associative D_2 desorption from Cu(211). We randomly choose a coverage, θ', and find pairs of (r, T_s) data corresponding to this θ' on all TPD curves starting with an initial coverage, θ_0, larger than θ'. Figure 4.7b) shows an Arrhenius plot of all ln r (i.e. ln $d\theta/dt$) versus $1/T_s$ for three random coverages indicated in Figure 4.7a).

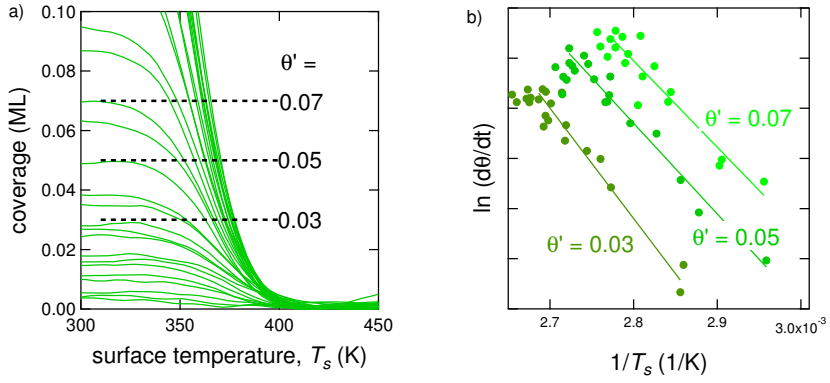

Figure 4.7: a) The remaining surface coverage during TPD versus time with three indicated remaining coverage for Cu(211). b) Exemplary Arrhenius plot for coverages indicated in panel a).

Figure 4.8 summarizes the obtained desorption energies and pref-

actors for Cu(111) (black circles) and Cu(211) (green squares) over the coverage range from 0 to $\sim$ 0.2 ML. The dashes lines in figure 4.8b) represents the average desorption energy and prefactors over this coverage range. They are $E_{des}^{111} = 74.4 \pm 1.3$ kJ/mol, ln $\nu^{111} = 25.9 \pm 0.4$ s^{-1}, $E_{des}^{211} = 72.0 \pm 1.1$ kJ/mol, and ln $\nu^{211} = 24.5 \pm 0.4$ s^{-1}.

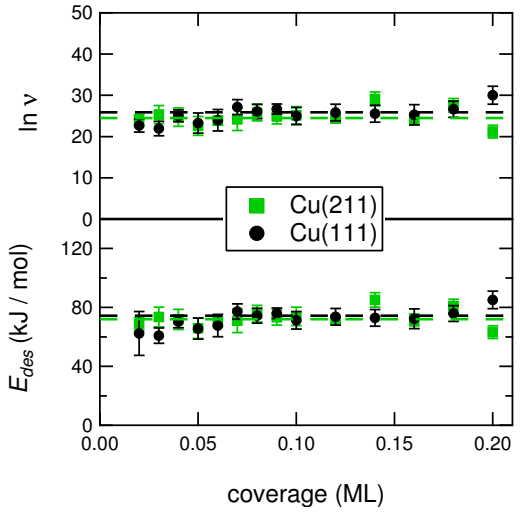

Figure 4.8: a) Prefactor and b) desorption energy obtained by complete analysis of TPD spectra for Cu(111) (black circles) and Cu(211) (green squares). Averages are indicated by dashed lines.

4.3.3 Determination of S_0 from TPD spectra

The integrated TPD spectra in figure 4.5 allow us to extract initial sticking probabilities that are considerably smaller than our KW limit. Figure 4.9 shows the results for Cu(211). We plot D_2 TPD integrals against a relative measure of the exposure for various expansion conditions. The relative measure of exposure is obtained by integrating the pressure increase in the chamber during the exposure to the pure beams. The slopes at the origin of the uptake traces in figure 4.5 are a relative measure of S_0 for each expansion condition. We use as an absolute reference the independently determined values of S_0 by the KW method for the higher temperature expansions. We use all of our values for S_0 obtained by the KW method to establish the best linear relationship with the slopes from figure 4.9. We then extrapolate to obtain values of S_0 for the lower incident energies, where we can not

obtain a signal using the KW method. Those values are indicated by open symbols in figure 4.4.

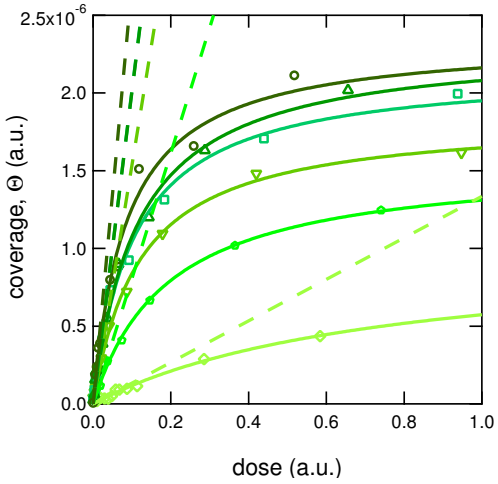

Figure 4.9: Coverage determined from integrating D_2 desorption from Cu(211) as a function of dose for molecular beams expanded at different nozzle temperatures. Increasing nozzle temperature and kinetic energy is symbolized by an increasingly darker shade of green. The solid lines are fits using a Langmuir adsorption model as described in the text. Dashed lines are the tangents at the origin for each fit and represent relative values of S_0.

4.3.4 Beam energy-dependent maximum coverage

The data in figure 4.9 suggest that for different expansion conditions, hence different most probable kinetic energies and kinetic energy distributions of our beams, the maximum attainable coverage, Θ_{max}, varies. This value is represented by the asymptotes of the individual curves. Increasing the beam's most probable energy leads to a higher asymptote. This type of behavior has been reported before for molecules experiencing a high barrier to dissociation, e.g. CH_4 on Pt(111)[80].

We fit our data in figure 4.9 using a simple Langmuir uptake model. The model assumes that there is no precursor state to dissociation. The molecule either dissociates upon impact or scatters back into the gas phase. Furthermore, desorption characteristics from our TPD spectra in figure 4.8 suggest that lateral interactions between adsorbed hydrogen atoms are weak, at least over the range 0 - 0.2 ML, for both Cu(111) and Cu(211). Therefore, we assume that the dissociation probability is not modified by lateral interactions. We integrate

$$\frac{d\Theta}{dt} = 2 \cdot S_0 \cdot \phi \cdot (1 - \frac{\Theta}{\Theta_{max}})^2 \tag{4.1}$$

with ϕ being the molecular beam flux at the crystal position and Θ_{max} the energy-dependent maximum coverage, to obtain

$$\Theta = \Theta_{max} \frac{S_0 \cdot (\phi \cdot t)}{S_0 \cdot (\phi \cdot t) + (\Theta_{max}/2)} \tag{4.2}$$

The fitting parameters are S_0 and Θ_{max}, while the dose equals the multiplication of the molecular beam flux ϕ, represented by the pressure rise in the UHV chamber, and time, t. The best fits to the data on the D_2 + Cu(211) system are shown as solid lines in figure 4.9.

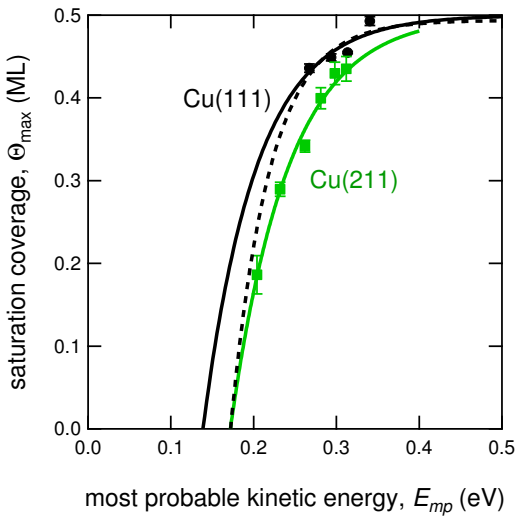

Figure 4.10: D_{ads} saturation coverage versus the most probable kinetic energy of the SMB used to dissociate D_2 on Cu(111) (black) and Cu(211) (green). The solid line through the data for Cu(211) is the best fit using the exponential functional form described in the text. The same best fit applied to the Cu(111) data only allowing an offset is shown as a solid black line. The dotted black line represents the best fit to Cu(111) data with the intercept at the energy axis fixed at identical value for Cu(211).

Figure 4.10 shows the dependence of Θ_{max} on the most probable kinetic energy of our molecular beams. The data are presented as symbols, i.e. black circles for Cu(111) and green squares for Cu(211). Error bars mark the uncertainty from the fits used to obtain the data. We have assumed that $\Theta_{max}^{(211)}$ and $\Theta_{max}^{(111)}$ for dissociating molecular hydrogen are both limited to 0.5 ML. Previous studies for Cu(111), Cu(110)

and Cu(100) all showed a 0.5 ML saturation coverage using atomic hydrogen sources[49, 81, 82]. As our surfaces are constructed from (111) facets with (100) steps, we consider our assumption of an absolute maximum coverage of 0.5 ML for Cu(211) to be reasonable. It allows us to use an absolute scale for Θ_{max} in figure 4.10. The data clearly show that higher maximum coverages are achieved for the atomically flat Cu(111) surface than for the highly stepped Cu(211) surface at any of the most probable incidence energies used in our molecular beam measurements.

As the data in figure 4.10 was obtained by fitting the maximum deuterium uptake using long exposures of the Cu surfaces to SMBs, the general trends may be interpreted to reflect how the minimum activation barrier to dissociation shifts upward with coverage. Unfortunately, the energy axis reflects the energy requirement in a rather indirect manner as our molecular beams have broad energy distributions. As the high energy tails of these distributions are likely responsible for the ultimately obtained coverage, we fit the data for Cu(211) in figure 4.10 using

$$\Theta_{max} = 0.5 \cdot (1 - e^{-(E_{kin} - E_{kin,0})/\beta}) \tag{4.3}$$

where $E_{kin,0}$ is the highest most probable kinetic energy that leads to no measurable dissociation. The value of β is a convoluted measure of how the minimum activation energy barrier shifts upward with D_{ads} coverage. A higher value of β represents weaker adsorbate-adsorbate interactions and a more constant activation barrier. In the absence of lateral interactions and a complete independence of the activation barrier on coverage, the data would be represented by a step function.

For Cu(211), the fit to the data is shown as a solid green line in figure 4.10. It intersects the energy axis at 0.172 eV. Allowing only a variation in $E_{kin,0}$, the same best fit to the Cu(111) data is shown as a solid black line. It is shifted by 34 meV. When fixing the cut off on the energy axis at the identical value for Cu(211), we obtain the dashed black fit for Cu(111). These two fits to the Cu(111) data represent two extremes. In the latter case, the minimum activation barrier to dissociative adsorption on the pristine surface is assumed to be the same for both surface structures. The coverage dependence of the minimum dissociation barrier is allowed to vary between the surfaces. In the former, the minimum activation barrier is taken to have the same dependence on coverage for both surfaces, but it is shifted to

Table 4.1: Classical activation barrier energies to dissociative adsorption reported in eV as calculated with the SRP48 functional for H_2 (D_2) on Cu surfaces and supercells presented in figure 4.1 at coverages of 0, 1/9, and 2/9 ML. Single values computed for 1/9 and 2/9 ML coverages are averaged values over all considered topologies of the H_{ads} overlayer. The actual energy range of the reaction barriers due to the different adsorbate overlayer structures is presented in brackets

surface	site	0 ML	1/9 ML	2/9 ML
Cu(111)	b_2	0.619	0.627 (0.603-0.642)	0.651 (0.623-0.677)
	t_2b	0.641	0.652 (0.627-0.701)	0.685 (0.609-0.815)
Cu(211)	b_2	0.640	0.662 (0.630-0.688)	0.684 (0.656-0.718)
	t_2	0.699	0.694 (0.680-0.731)	0.687 (0.657-0.722)

start at a lower value for Cu(111).

4.3.5 Coverage-dependent dissociation barrier from theoretical calculations

The results from our DFT calculations of reaction barriers are summarized in table 4.1 in eV. It lists the minimum reaction barrier energies calculated for the dissociation sites also shown in figure 4.1 for the (3×3) unit cell of Cu(111) and (3×1) unit cell of Cu(211) for the pristine surface (0 ML). The values for Cu(111) and Cu(211) are consistently $\sim$ 20 meV lower than those obtained for identical geometries on smaller unit cells as presented in our previous study[70]. This finding is in agreement with previous DFT calculations on the dependence of the reaction barrier height of H_2 on Cu(111) on the coverage that yielded generally lower barriers for smaller coverages (larger supercells)[83]. Specifically for the change of the supercell size from (2×2) to (3×3), the computed reaction barrier was reduced by up to 25 meV, depending on the computational setup used. Also listed in table 4.1 are single barrier energies for pre-covered surfaces at 1/9 and 2/9 ML obtained as average over all considered H_{ads} overlayer structures and the corresponding range of barrier energies according to the different topologies of the different adsorbate overlayers we have taken into account in the computations. For simplicity, we represent the average barrier energies as standard average values. They therefore do not capture potential effects arising from finite temperatures as, for example, thermodynam-

ical mean energy values would do. We also neglected coverage situations that would lead to adsorbed atoms in neighboring HCP and FCC sites, and, therefore, strongly repulsive interactions. According to figure 4.1a), transient H_2 dissociating at the edge of cell 1 and 7, respectively, would experience considerable interactions with H_{ads} positioned at the HCP sites in cell 7 and 8, and the FCC sites at cell 1 and 3 due to the employed periodic boundary conditions. The activation barrier for this situation is 0.951 eV, i.e. much higher than all other situations not leading to neighboring adsorbed H atoms. The latter generally show minimum energy barriers in the range 0.6 - 0.7 eV. All situations leading to neighboring H atoms show barriers near 1 eV.

The table shows several noteworthy features. First, the averaged minimum activation barriers generally rise very modestly with coverage for all dissociation geometries on Cu(111) and Cu(211), except for Cu(211)'s t_2 site. There the activation barrier energy drops with coverage. Second, the lowest values found for dissociation for particular geometries, i.e. the low end of the indicated ranges, may not even show any significant rise in the minimum reaction barrier. The observation of lower barriers at 1/9 and 2/9 ML appears at present loosely connected with the specific coverage configurations, that is, steric hindrance effects as discussed in refs. [84, 85] seem to be less important for the variation of the reaction barriers than resulting changes in the electronic structure. Third, only Cu(211)'s t_2b site shows a significant dependence on the exact adsorption sites of the 2 H_{ads} atoms with 0.2 eV in between the most and least favorable geometries. All other ranges show variation around 0.05 or 0.07 eV.

4.4 Discussion

We start our discussion with the comparison of dissociative sticking probabilities for Cu(111) as shown in figure 4.3. While our results compare well to those reported by Winkler and coworkers [49, 51], they far exceed those reported by Auerbach and coworkers for D_2[53] and H_2 [55]. Considering the excellent agreement between theoretically predicted sticking probabilities and the latter experimental data, as shown by Díaz et al.[34], an experimental difference must cause our sticking data to be higher. The origin of the discrepancy between Winkler's and Auerbach's data was pointed out by Díaz et al. When

convoluting the energy-resolved sticking probabilities produced by theory with the experimental energy distributions, results matched both experimental reports. Higher sticking probabilities found in the case of broader energy distributions result from poorer kinetic energy cooling in the supersonic expansion. Our sticking probabilities are nearly identical to those published by Berger et al. [51] for comparable conditions when we correct for the offset in the detection of our nozzle temperature (see table S6 in ref. [70]). As we have also previously determined nearly identical scaling between the kinetic energy and T_n (i.e. 2.53k) for our experimental apparatus as reported by Winkler (∼2.5k), and that this value is smaller than the one reported by Auerbach (∼2.65k), we conclude that the discrepancy with Auerbach's data is a result of poorer cooling in our molecular beam expansion.

We also compare our TPD spectra for Cu(111) to those reported by Anger et al. [49] for the same surface. With a ramp rate of 3 K/s, they find a single desorption feature with peak desorption temperatures increasing from ∼ 320 to 360 K with decreasing initial coverage. Their spectra show clearly overlapping trailing edges. These peak values and the TPD shapes are thus very similar to ours as presented in figure 4.5. The determined desorption energies in the range of 0 to 0.20 ML are in both cases coverage-independent and quantitatively similar. Our value of 74.5 kJ/mol compares reasonably well to the desorption energy we extract from their publication, 87 kJ/mol, as determined by the same analysis method. Frequency factors in this coverage regime were reported only from a leading edge analysis of TPD spectra [86], and show larger scatter that our data reported in figure 4.8a). Quantitatively, they agree reasonable well, though. Taking the different units for coverage into account, they find $^{10}\log\nu \sim 11.8$ where we find 11.2 for Cu(111). From the comparison of adsorption and desorption, we conclude that our data for this surface are quantitatively consistent with previous experimental reports that used the same experimental techniques and conditions, and analysis of data.

Turning to our results for Cu(211), the most remarkable finding is that the sticking probability of D_2 is larger on Cu(111) than on Cu(211). It may be considered of relevance that dissociation on the (111) plane strongly depends on the impact angle between the molecular beam and the surface normal[49, 51]. The angular dependence of the sticking probability, S, relates to the desorption probability, D, and is described by the equation:

$$\frac{S(E,\theta)}{S(E,0^\circ)}cos\theta = \frac{D(E,\theta)}{D(E,0^\circ)} \approx cos^n\theta \tag{4.4}$$

where n for Cu(111) is approximately 6 in the energy regime that we have probed[49, 51]. The angle between the (111) facet and the surface normal of the (211) plane is 19.5°. If sticking only occurs on the (111) facets of the (211) surface, the local sticking probability would be ∼0.75 times the value found for Cu(111). Only when assuming that the step area is unreactive and occupies approximately one third of the surface area, the weighted average reactivity over the (211) unit cell validates our experimental ratio of ∼0.5 for S_0^{211} and S_0^{111}. Although this may appear to be an acceptable explanation, the assumed lack of reactivity of the Cu A-type step would be highly surprising, especially since steps are generally expected to increase reactivity through lowering activation barriers in the dissociation of diatomics[87]. Many supersonic molecular beam experiments for hydrogen dissociation on stepped surfaces of other transition metals have supported this view[26, 28–30, 88].

Our recent combined theoretical-experimental study [70] explains the counterintuitive result. It showed that activation barriers on various locations within the unit cell of Cu(211) for D_2 dissociation are $30-90$ meV higher than on Cu(111) surface. The difference is observed again in the new results presented for 0 ML coverage in table 4.1. On Cu(111), the b_2 bridge site has the lowest dissociation barrier of ∼0.62 eV. The similar b_2 bridge site on the short (111) terrace, positioned near the downward edge, and the t_2b sites are found to have the lowest barriers for Cu(211), i.e. ∼0.64 eV. The barrier at the bottom of the edge is found to have a barrier near 0.70 eV. Based on the similarity of the current new calculations for the (3×3) unit cell for Cu(111) and (3×1) unit cells for Cu(211) and the previously reported values, the previous conclusions regarding the differences in reactivity of these surfaces are expected to hold. Energy dependent values for S_0 were calculated and agreed rather well with experimental results when taking the broad energy distribution of experimental molecular beams into account. However, the computed reactivity overestimates the absolute experimental value slightly. That difference should be reduced by the lower barriers reported in table 4.1 while maintaining higher reactivity of Cu(111) compared to Cu(211). Our new data on sticking at low incidence energies shown in figure 4.4 and extracted from TPD measurements allows to compare experiment and theory on a wider energy

range. This may help to determining the role of quantum mechanical tunneling for reaction and to further validate the performance of the approximations used in the dynamics calculations on sticking.This includes the Born-Oppenheimer static surface approximation and the electronic structure theory to compute the H_2 + Cu(211) interaction potential.

Our experimental data for desorption adds information regarding the effect on the potential energy surface governing the H_2/Cu interaction when disrupting the (111) plane with an A-type step. The higher dissociation barrier for Cu(211) may result from weakened binding of H(D) atoms in the zero-coverage limit, as illustrated in figure 4.11. From linear scaling between the binding energy, E_b, and the activation energy to dissociative adsorption, E_{act}[87], the difference in the desorption barrier for Cu(111) and Cu(211), ΔE_{des}, should be similar to the difference in activation barriers for these two surfaces, ΔE_{act}. From figure 4.8b), this appears to be the case. We found averaged desorption barriers over the 0 to 0.2 ML range for Cu(211) and Cu(111) differing by 2.4 kJ/mol (25 meV).

Our previous trajectory calculations simulating beam conditions with an incidence energy of 34 kJ/mol showed that molecules dissociated over different barriers positioned across the unit cell. Only ∼50% of the reaction is mediated over the step edge area. In Ref. [70], we have predicted that reaction is likely also over other regions, namely at the b_2 site located on the (111) terrace and at the t_2 site located at the bottom of the step. This may also have consequences for the desorption process, as discussed in the following. The average value of the activation energies at zero-coverage for the three sites listed given in table 1 is 0.652 eV, taking into account that the t_2b and the b_2 sites appear twice and the t_2 site only once in the (211) unit cell. This leads to an increase of the average activation energy by approximately ΔE_{act} = 33 meV in comparison to transition state energy of the H_2 + Cu(111) system. This compares well to the ΔE_{des} ∼25 meV found from TPD fitting. It also compares well to the difference between cut off values in figure 4.9. The difference in the energy requirement at the zero-coverage limit to obtain dissociation was found to be 34 meV when assuming that the activation barrier distribution was simply shifted upward for Cu(211) compared to Cu(111). The latter assumption is supported by the findings in table 4.1 when comparing the difference between the averaged barrier heights for Cu(211) with Cu(111) for pre-

coverages of 1/9 and 2/9 ML. The difference remains on the order of 35-40 meV, supporting the lateral shift, and not the option provided by the dashed line in figure 4.9. This finding is again consistent with a (near) invariance of the desorption energy found in figure 4.8 over the same coverage regime. Although the effects on the activation barrier to dissociation and the binding energy by introducing the A-type step to the (111) plane are small compared to the dissociation barrier itself ($\sim 5\%$), our new experiments detect them with reasonably consistent absolute values. They are on the order of several tens of meV. These values are also in quite good agreement with the new calculations of the coverage dependent barrier heights to dissociation.

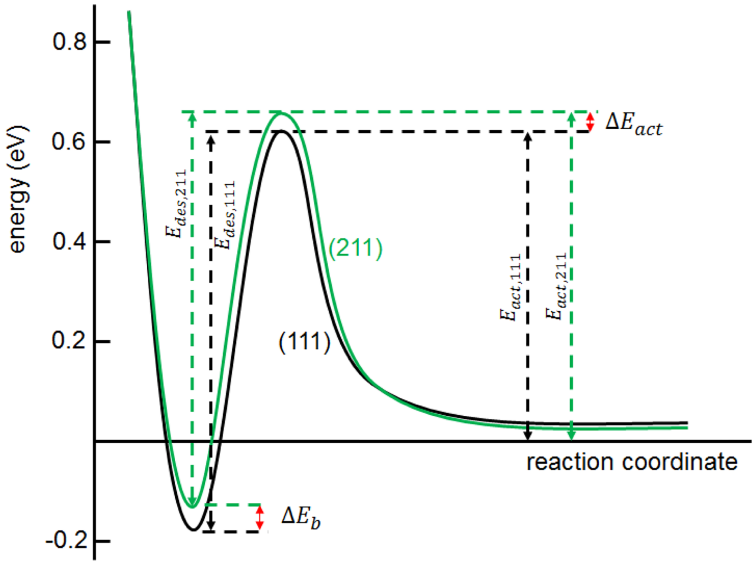

Figure 4.11: Schematic illustration of the dimensional PES for dissociation on Cu(111) (black) and Cu(211) (green) with indications of the activation barrier heights for dissociation, $E_{act,n11}$, and recombinative desorption, $E_{des,n11}$, as vertical dashed arrows, and the differences in binding energy, ΔE_b, and activation barrier to dissociation, ΔE_{act}.

We finally address whether the differences between Cu(211) and Cu(111) in adsorption and desorption can be linked to the shoulder at lower temperature observed for high coverages in the TPD spectra of figure 4.5 and modeled in figure 4.6. A small shoulder on the low temperature side of the main desorption feature has been reported before in the studies of H atoms incident on Cu(110)[49, 82] and H/D on Cu(111)[57]. In all cases, an atomic hydrogen beam was used to create

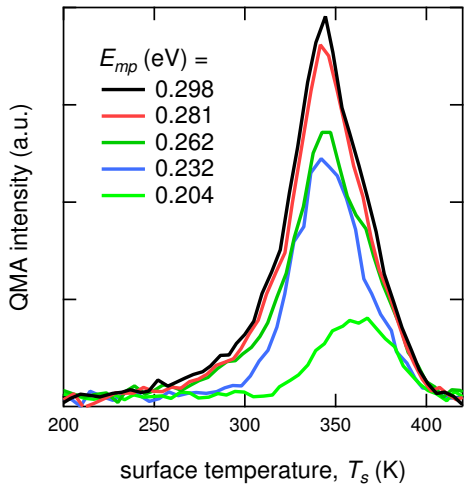

Figure 4.12: TPD curves for saturation coverages obtained using beams with increasing most probable kinetic energy.

some coverage of H_{ads}. The shoulder was consistently ascribed to desorption resulting from resurfacing of subsurface hydrogen. In the study by Rettner and Auerbach [57], this shoulder also did not saturate with increasing exposure and increased to an amount equivalent to 1.5 ML. The shoulder was in previous studies on low Miller index Cu surfaces never reported when using molecular hydrogen. We find it only in TPD spectra from the Cu(211) surface, excluding that it results from a small concentration of deuterium atoms in our highest temperature expansions beam. Had the highest nozzle temperatures led to presence of atomic H(D) in our beams, we should have observed the desorption feature also for Cu(111). As this is not the case, we conclude that it is a new feature associated with the occurrence of the A-type step of the Cu(211) plane. Its size compared to the main desorption feature is small, accounting for only $\sim 15\%$ of the total desorption yield. Oddly, it appears well before saturation of the main desorption feature. In figure 4.12 we have gathered TPD spectra obtained from D-saturated Cu(211) obtained at different nozzle temperatures. The shoulder peak clearly appears when the most probable incident kinetic energy of our beam equals 0.262 eV. However, at this energy, we are not yet close to the assumed limiting coverage of 0.5 ML. With higher incident energy, mostly the main desorption feature continues to increase. We interpret this to signal that a particular dissociation site on Cu(211) exists

- one not present on Cu(111) - and correlated to a significantly lowered desorption energy, as apparent from the Runge-Kutta fit ($E_{des} \sim$ 52 kJ/mol compared to 75.5 for the main feature). The site may be dynamically constrained - associative desorption occurs with limited lateral mobility. This may occur, for example, at sites at the bottom of step edges, e.g. the t_2 site, where diffusion barriers can be highly anisotropic. Dissociation at this site is also consistently found to have a higher barrier than the t_2b and b_2 sites on Cu(211). We note, though, that previous combined theoretical-experimental studies have shown that great care must be taken in relating hydrogen adsorption and desorption sites to desorption peaks in TPD spectra of complex surfaces. [89]

4.5 Conclusion

From our new study of hydrogen adsorption and desorption we find consistent trends regarding the effect of introducing A-type steps to the (111) plane of Cu. Whereas the lowered coordination of step atoms usually leads to lowering of dissociation barriers by increasing the binding energy, we find the opposite behavior here. A-type steps cause a - so far unique - upward shift in the distribution of activation barriers to adsorption and a downward shift in barriers to desorption. The effect is small in comparison to the absolute barrier heights, on the order of 5%, but it is clearly detectable. Furthermore, the barrier distributions are weakly dependent on hydrogen pre-coverage and saturation coverages are shown to depend on incident energy. Lateral interactions between adsorbed hydrogen atoms must be weak, especially in the lower coverage regime. Although the latter may be expected, the lowering of reactivity toward dissociation of a diatomic by introducing monoatomic steps surely is not.

During final stages of the preparation of this manuscript, results of a new state-resolved experimental study on molecular hydrogen desorption following atomic permeation through Cu single crystals appeared [90]. From application of the principle of detailed balance to their results, the authors come to the same conclusion regarding the reactivity of the clean Cu(111) and Cu(211) surfaces for three molecular hydrogen isotopologues. The stepped surface shows higher activation barriers and a broader distribution than the Cu(111) surface. At first

glance, the difference in activation barriers for direct activated adsorption onto the clean surfaces seems to agree quantitatively reasonably well with the barriers extracted here in our manuscript from TPD measurements. Averaged over the first J states, they report a shift in barrier distribution of several tens of meV for D_2. A second mechanism to adsorption, extracted from their desorption data, which shows a characteristic negative dependence on incident energy, lies outside the energy regime probed in our adsorption measurements. The results of this new study are encouraging to us. This independent work is based on a different experimental technique and definitively confirms our earlier and present conclusion of Cu(211) being less reactive then Cu(111) for hydrogen dissociation.